AMERICAN SOCIETY FOR MICROBIOLOGY | mSystems®

RESEARCH ARTICLE

Identification of Cyclic-di-GMP-Modulating Protein Residues by Bidirectionally Evolving a Social Behavior in *Pseudomonas fluorescens*

Collin Kessler,[a] Wook Kim[a]

[a]Department of Biological Sciences, Duquesne University, Pittsburgh, Pennsylvania, USA

ABSTRACT Modulation of the intracellular cyclic di-GMP (c-di-GMP) pool is central to the formation of structured bacterial communities. Genome annotations predict the presence of dozens of conserved c-di-GMP catalytic enzymes in many bacterial species, but the functionality and regulatory control of the vast majority remain underexplored. Here, we begin to fill this gap by utilizing an experimental evolution system in *Pseudomonas fluorescens* Pf0-1, which repeatedly produces a unique social behavior through bidirectional transitions between two distinct phenotypes converging on c-di-GMP modulation. Parallel evolution of 33 lineages captured 147 unique mutations among 191 evolved isolates in genes that are empirically demonstrated, bioinformatically predicted, or previously unknown to impact the intracellular pool of c-di-GMP. Quantitative chemistry confirmed that each mutation causing the phenotypic shift either amplifies or reduces c-di-GMP production. We identify missense or in-frame deletion mutations in numerous diguanylate cyclase genes that largely fall outside the conserved catalytic domain. We also describe a novel relationship between a regulatory component of branched-chain amino acid biosynthesis and c-di-GMP production, and predict functions of several other unexpected proteins that clearly impact c-di-GMP production. Sequential mutations that continuously disrupt or recover c-di-GMP production across discrete functional elements suggest a complex and underappreciated interconnectivity within the c-di-GMP regulome of *P. fluorescens*.

IMPORTANCE Microbial communities comprise densely packed cells where competition for space and resources is fierce. Aging colonies of *Pseudomonas fluorescens* are known to repeatedly produce mutants with two distinct phenotypes that physically work together to spread away from the overcrowded population. We demonstrate that the mutants with one phenotype produce high levels of cyclic di-GMP (c-di-GMP) and those with the second phenotype produce low levels. C-di-GMP is an intracellular signaling molecule which regulates many bacterial traits that cause tremendous clinical and environmental problems. Here, we analyze 147 experimentally selected mutations, which manifest either of the two phenotypes, to identify key residues in diverse proteins that force or shut down c-di-GMP production. Our data indicate that the intracellular pool of c-di-GMP is modulated through the catalytic activities of many independent c-di-GMP enzymes, which appear to be in tune with several proteins with no known links to c-di-GMP modulation.

KEYWORDS biofilms, cyclic-di-GMP, diguanylate cyclase, eubacteria, experimental evolution, microbial communities, secondary metabolism, social interaction

Microbes utilize diverse signaling mechanisms to adapt and respond to a dynamic environment. Cyclic di-GMP (c-di-GMP) is a ubiquitous secondary messenger in bacteria, and high intracellular levels of c-di-GMP characteristically repress flagellar motility while stimulating the expression of biofilm-formation genes (1–4). Numerous c-di-GMP binding proteins and riboswitches respond to intracellular levels of c-di-GMP to also regulate cellular morphology, virulence factors, antibiotic production, and the cell cycle (5, 6). C-di-GMP

Editor Ákos T. Kovács, Technical University of Denmark

Address correspondence to Wook Kim, kimw1@duq.edu.

The authors declare no conflict of interest.

Received 2 August 2022
Accepted 13 September 2022
Published 3 October 2022

is synthesized from two molecules of GTP by a diguanylate cyclase (DGC) and hydrolyzed by a phosphodiesterase (PDE) (1). DGCs and PDEs are identified by the GGDEF and EAL/HD-GYP domains, respectively, and there are also hybrid proteins with both DGC and PDE functions (7, 8). However, relatively little is known about other functional domains, if any at all, in most DGCs/PDEs.

Pseudomonas spp. typically possess greater than 50 predicted DGCs or PDEs (9), but systematically knocking out independent genes appears to have relatively little impact on the intracellular c-di-GMP pool (9). Each enzyme could collectively influence the total intracellular pool (10) or independently carry out a subcellularly localized role (11). Specific signaling pathways or regulators have been characterized to independently regulate several DGCs and PDEs (12–19), and some have been demonstrated to be under allosteric control, where a certain range of c-di-GMP levels either initiate or prevent enzymatic activity (20–24). However, the function of the vast majority of bioinformatically predicted DGCs and PDEs has not been empirically validated, and their regulatory mechanisms remain entirely unknown (25).

Experimental evolution studies in *Pseudomonas* and *Burkholderia* readily capture diverse mutations that impact biofilm formation, including those that alter c-di-GMP levels (26–28). We have previously described the bidirectional evolution of mucoid (M) and dry (D) colony phenotypes in *P. fluorescens* Pf0-1, which appears to occur exclusively through c-di-GMP oscillation (29). An aging colony of M cells repeatedly produces spreading fans at the perimeter, which comprises the original M cells along with new D mutant cells that produce a dry and wrinkly colony morphology on their own. Additionally, an aging colony of D cells also repeatedly generates spreading fans, which comprise the original D cells along with a new mutant that appears phenotypically identical to the ancestral M. This bidirectional selection of M and D phenotypes occurs continuously because M and D cells self-organize in space and physically work together to spread out from the nutrient-poor and crowded conditions of dense colony growth, and neither type is capable of spreading out on its own. Genetic analyses of five evolved isolates revealed characteristic mutations in *wsp* genes to suggest that c-di-GMP production is likely elevated in D and reduced in M (29).

Here, we carry out a large-scale parallel evolution experiment using the bidirectional M-D system to identify 147 unique mutations in genes that are empirically demonstrated, bioinformatically predicted, or previously unknown to impact c-di-GMP levels. We expand the current model of c-di-GMP production by the Wsp signal transduction system and identify unique missense mutations outside the conserved catalytic domain of numerous DGCs that stimulate or reduce enzymatic activity. We also describe proteins with no previous associations to c-di-GMP production that appear to influence the activity of several DGCs, including a regulatory component of the branched-chain amino acid (BCAA) biosynthesis pathway. Lastly, we model the interconnectivity of the c-di-GMP regulome by mapping sequential mutations that disrupt or recover c-di-GMP production across functionally discrete systems.

RESULTS AND DISCUSSION

Bidirectional evolution of mucoid and dry phenotypes occurs through intracellular c-di-GMP pool oscillation. The bidirectional selection of mucoid (M) and dry (D) phenotypes occurs continuously in our experimental system (29) because neither type is capable of spreading out on its own, but a colony of initially mixed M and D cells readily spreads out in a radial pattern without requiring additional mutations (Fig. 1A). With the expectation that a large-scale utilization of this experimental evolution system could identify diverse mechanisms of c-di-GMP modulation, we initially set up 25 parallelly evolving lineages of the common ancestral M isolate, which is also referred to as M0. We randomly picked evolved isolates of D from M0, and each D isolate (D0) represents the first branching point and the ancestor of its respective lineage (Fig. S1). We then randomly picked several evolved isolates of M from independent D0 isolates, and they are referred to as M1; D1 evolved from M1, M2 evolved from D1, D2 evolved from M2, and so on (see Materials and Methods for a detailed description of the experimental procedures). We also established additional lineages with genetically engineered ancestral strains, as described below, to represent 33 lineages in total. As anticipated, we observed bidirectional transitions between M and D phenotypes across all lineages. In sum, we evolved over 600 isolates, analyzed genome sequences of 191 isolates, and

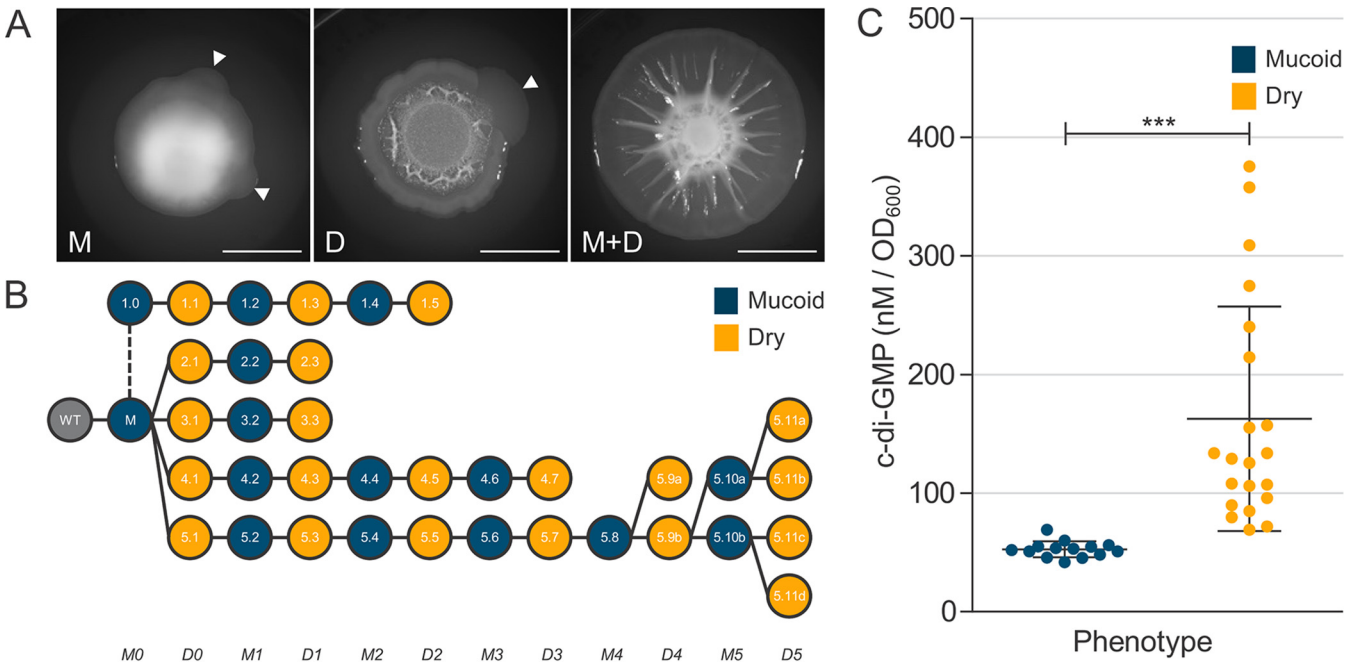

FIG 1 Bidirectional evolution of M and D phenotypes are c-di-GMP dependent. (A) Colony morphologies of the ancestral mucoid (M, left) and dry (D, middle) isolates after 4 days of growth. Arrows indicate the emergence of spreading fans that contain the respective parent and a new mutant with the opposite phenotype. The spreading phenotype is readily produced by artificially mixing M and D isolates (right, scale bar = 10 mm). (B) Phylogeny of isolates in select lineages colored by phenotype and corresponding colony morphologies are shown in Fig. S2. The numbers indicate the IDs of the evolved isolates as shown in Table S1. Isolate 1.0 was constructed from the ancestral M isolate to lack the *wspC* gene, which encodes a methyltransferase, known to activate the Wsp system. Each isolate was sampled from naturally emerging fans from their respective parent colony with the opposite phenotype. This phylogeny depicts the bidirectional transitions between mucoid and dry states, which we show are c-di-GMP dependent. (C) C-di-GMP levels of evolved isolates. C-di-GMP was quantified through LC-MS/MS and is reported as nM per OD_{600}. Samples are categorized by phenotype, and we report the triplicate mean ± standard deviation (SD) for each phenotypic classification: mucoid $n = 14$ and dry $n = 21$ (***, Student's t test $P < 0.001$).

quantified c-di-GMP in a subset of 56 isolates. Only the sequenced isolates within in each lineage are depicted in Fig. S1 in the supplemental material and summarized in Table S1. We also employed a numerical nomenclature to distinguish isolates from independent lineages. The first number represents the lineage number, and the second number represents the chronology of sequential transition steps. For example, 5.1 represents the first D0 isolate that evolved from M0 in lineage 5, and 5.2. represents the M1 isolate that evolved from D0, and so on.

Remarkably, we primarily detected a single mutation associated with each phenotypic transition, with few additional silent mutations across all genome sequences. Genome sequencing of successive isolates within each lineage provided an internal control, which confirmed the exclusive presence of the respective preceding mutations. Among the 147 unique mutations detected, 81 mutations were in *wsp* genes and 66 mutations were in other genes including those that are hypothetical. Motility assays showed that all D isolates were nonmotile and all M isolates were motile as expected, and liquid chromatography tandem mass spectrometry (LC-MS/MS) quantification confirmed that c-di-GMP was elevated in all D isolates relative to their respective parent M isolate (Table S1). Notably, many mutations in non-*wsp* genes sequentially flanked specific mutations in the Wsp signal transduction system, the most extensively studied c-di-GMP regulatory system in *Pseudomonas* spp. (19). Several missense mutations observed in Wsp proteins identified in this study overlap comparable mutations from various *Pseudomonas* and *Burkholderia* studies that we had previously compiled from the literature (19) (Fig. 2). However, the vast majority of mutations identified in this study had never been observed, and many occur outside functionally annotated domains. The data presented in Fig. 2 represent the most comprehensive record of functionally important residues of the Wsp system to date and empower our predictions of mutation consequences. We first focus on sequential mutations in the Wsp system to reveal both predictable and surprising evolutionary innovations to modulate c-di-GMP production. For the sake of an

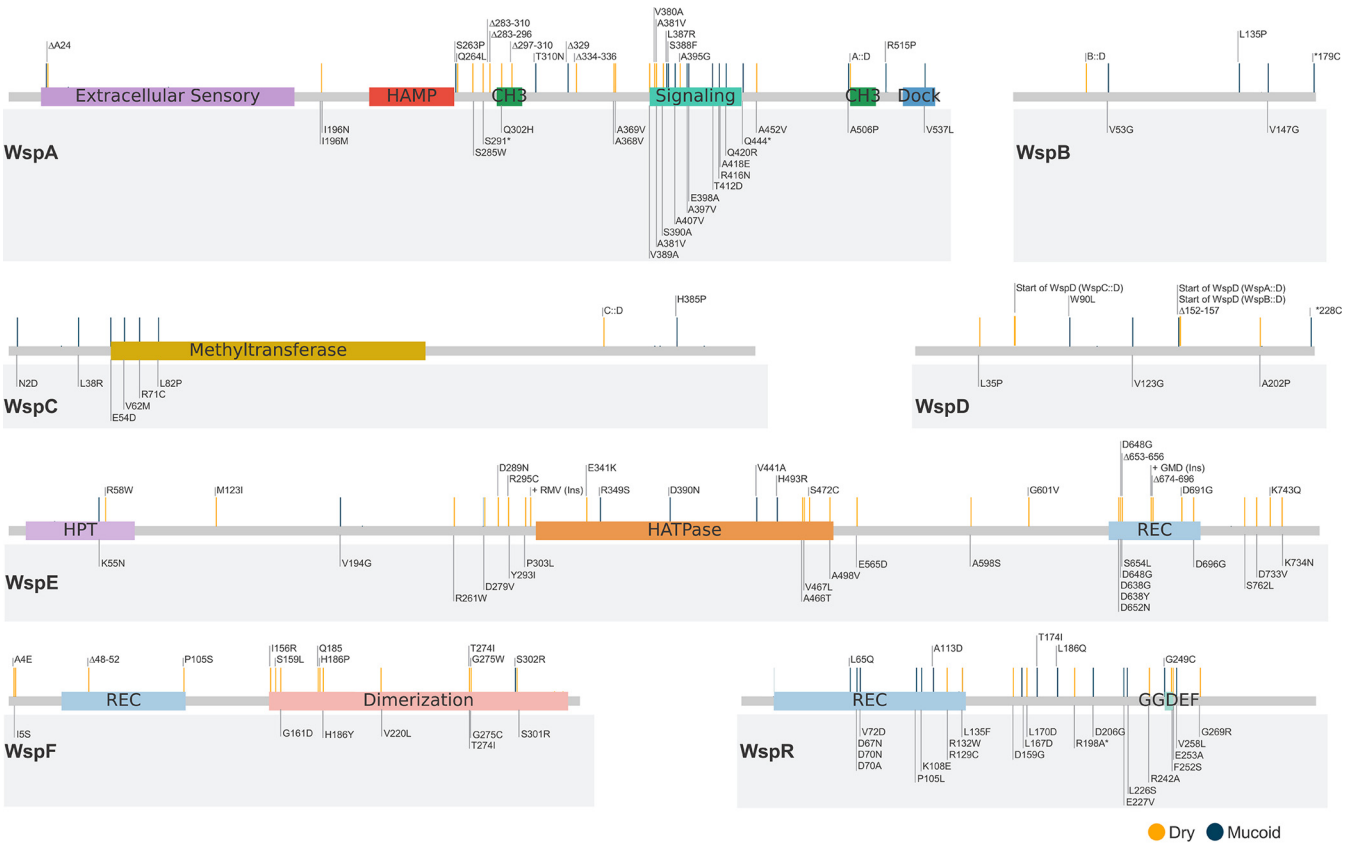

FIG 2 Alignment of our missense and in-frame deletion mutation data with previously annotated mutations in the Wsp system. Individual Wsp proteins are shown with their functional domains that were derived from CDD (NCBI), Prosite, or homology to the *E. coli* chemotaxis system (HAMP, transmembrane relay domain; CH_3, methylation site; HPT, histidine phospho-transfer domain; HATPase, histidine kinase ATP binding domain; REC, phosphoreceiver domain). Only the missense and in-frame mutations identified in this study are shown, and they are mapped to the consensus sequence of each Wsp protein (19). Previously annotated mutations (19) are shown in the gray box below each protein. Mutations indicated in the gray box are annotated to represent specific residue positions that were affected in the respective protein sequence of a given organism, but the gray horizontal bars indicate their actual positions within the consensus sequence. Therefore, the horizontal bar locations of the mutations identified in this study are directly comparable to previously identified mutations through the consensus sequence. Mutations that stimulate c-di-GMP production are indicated by orange horizontal bars, and those that reduce c-di-GMP production are indicated by blue horizontal bars.

accessible narrative, we will primarily refer to five simplified lineages (Fig. 1B), with corresponding c-di-GMP measurements (Fig. 1C) and colony morphologies (Fig. S2).

Diverse mutations dynamically rewire signal flow to produce a spectrum of functional states of the Wsp signal transduction system. The Wsp signal transduction system was first reported 2 decades ago in *P. fluorescens* (30) and continues to serve as the primary model system of c-di-GMP regulation in pseudomonads. The Wsp system comprises seven proteins encoded in a monocistronic operon under the control of an unidentified transcriptional regulator (31), and the current functional model is based on a combination of empirical studies and predictions based on homologies to the chemotaxis system in *Escherichia coli* (19). The main difference with the latter is that the signal cascade is initiated by the extracellular sensory domain of WspA detecting surface contact (32, 33) to ultimately drive c-di-GMP production by the DGC WspR (Fig. 3). Given that a mutation in any one of the seven Wsp protein-coding genes could potentially increase or decrease c-di-GMP production through WspR, we expected *wsp* genes to be a common target in our parallel evolution experiments. Indeed, the vast majority of the first transitions from the ancestral M to D occurred through either a missense or an in-frame deletion mutation in *wsp* genes (Table S1).

Across our subset of five lineages (Fig. 4), initial mutations appear to artificially activate WspA, followed by surprisingly similar patterns of sequential mutations in various *wsp* genes to oscillate c-di-GMP production. Lineages 2 and 3 began with the first respective D isolate possessing a unique in-frame deletion that partially spans the predicted methylation helices of WspA. Lineage 5 began with a missense mutation in the phosphoreceiver domain of

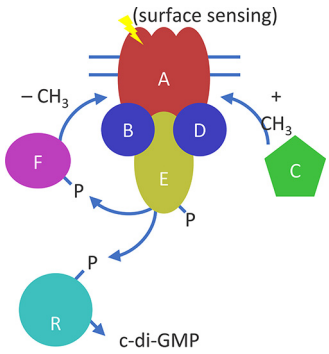

FIG 3 Functional model of the Wsp signal transduction system. The Wsp system in *P. aeruginosa* responds to surface contact to ultimately produce c-di-GMP. (CH3, methyl group; P, phosphoryl group). Homology with the chemotaxis system predicts that once WspA is stimulated by surface contact, it undergoes a conformational change to expose cytosolic methylation helices that are necessary for signal transduction (34). The methyl-transferase WspC is then predicted to dock at the 5′ tail of WspA and methylate the WspA trimer-of-dimers complex (58). The signal is then relayed through the coupling proteins WspB and WspD, and subsequently to WspE, which functions as a histidine kinase (59). WspE phosphorylates the DGC WspR to stimulate c-di-GMP production (60). Simultaneously, WspE phosphorylates the methyl-esterase WspF, which demethylates WspA and terminates the signaling cascade (31). Significant work has been carried out to characterize the biochemical functions of WspE and WspR in particular, and WspE is a common mutational target in clinical settings (19). More recently, studies have begun to explore the functional role of WspA during signal activation and subcellular localization, revealing that both properties are dependent on WspB and WspD proteins (32, 61). These studies also suggest that WspB and WspD likely possess unique functions, but they remain unresolved.

WspF (P105S), which likely disrupts its methyl-esterase activity to keep WspA in an activated state. This activation is undone in the following M isolate by an in-frame deletion in *wspA* that removes the amino acid residue S329, and then c-di-GMP production is restored again in the next D isolate through an in-frame deletion of residues 283 to 296 in WspA. This deletion falls within the same deleted region as those observed in lineages 2 and 3 (Fig. 2, Fig. 4). Although methylation of WspA remains to be empirically demonstrated, its predicted methylation helices clearly have a functional role in Wsp signaling, as they were commonly mutated to activate c-di-GMP production (Fig. 2). Based on our mutation data and homologies to Tsr-methylation in the chemotaxis system of *E. coli* (34), we predict that the residues Q285, E292, E299, Q502, and E512 are methylated and the deletion of these sites mimics a methylated state. We also set up an independent lineage to commence with an engineered Δ*wspC* M isolate (Fig. 4, isolate 1.0), under the expectation that the deletion of *wspC* would steer downstream mutations away from the Wsp system. However, we detected a missense mutation within the signaling domain of WspA (A381V) in the first D progeny isolate 1.1, and the same A381V mutation was previously observed in an independently evolved D isolate with an unaltered *wspC* gene (29). We detected additional missense mutations in WspA's signaling domain to independently stimulate c-di-GMP production (Fig. 2), which likely bypass the methylation requirement to activate WspE.

Mutations that stimulate WspA were typically followed by a missense mutation in WspB, WspD, or WspE (Table S1). A missense mutation in WspD (W90L) in lineage 2 reduced c-di-GMP production like the WspB (L136P) mutation in lineage 1 (Fig. 4). The functional roles of WspB and WspD in signal relay are loosely modeled after homology to CheW of *E. coli*, which remains the least characterized protein in the chemotaxis system. Mutations in CheW that successfully disrupt signal transduction are largely limited to five unique amino acid clusters that situate on the protein surface and are essential for the docking of CheW to Tsr (WspA homolog) (35). WspB and WspD also possess six and seven highly conserved amino acid clusters, respectively (19). Our WspB L135P and WspD W90L mutations fall within these conserved clusters that likely situate on the surface of WspB and WspD and natively act as docking sites for WspA and WspE to permit signal relay. We also observed additional missense and in-frame deletion mutations in WspB and WspD that independently impact c-di-GMP production (Fig. 2, Table S1), confirming that both WspB and WspD are necessary for Wsp signal transduction through domains and interactions that remain to be characterized.

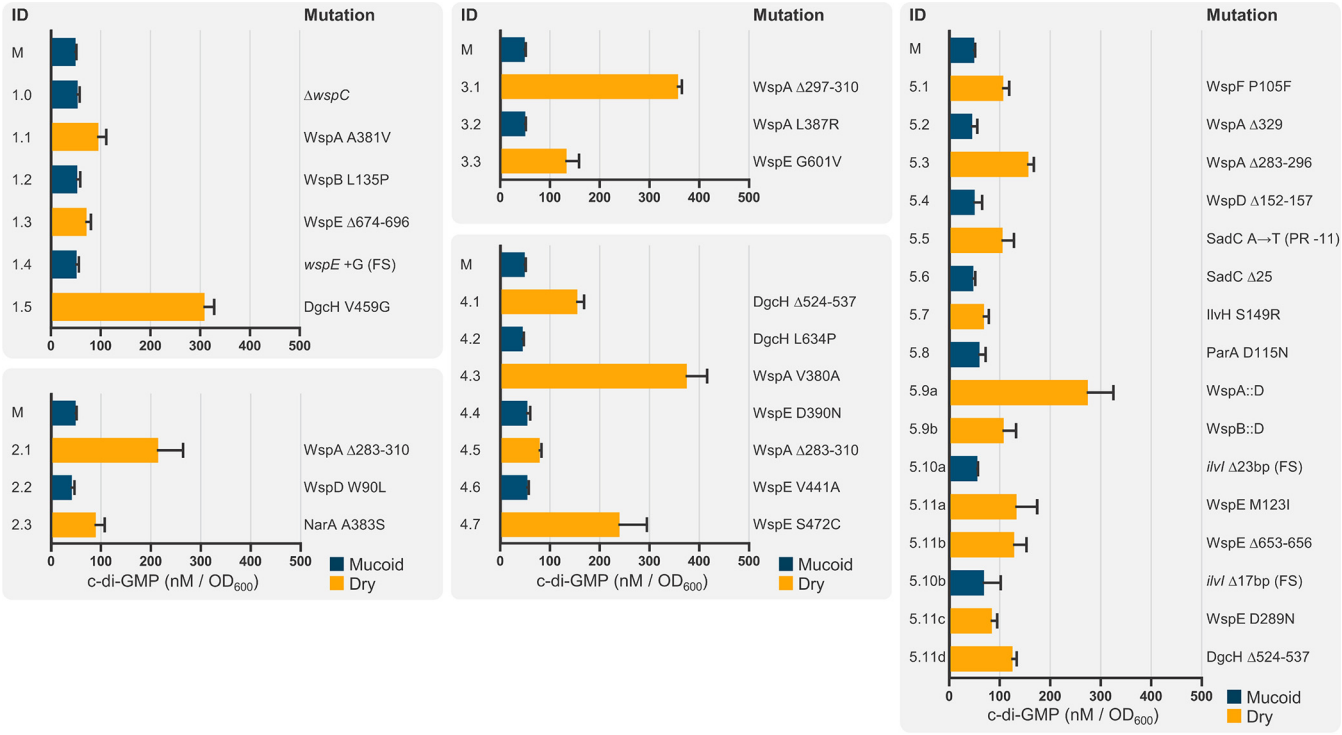

FIG 4 C-di-GMP oscillates between all M and D phenotypic transitions. C-di-GMP was quantified via LC-MS/MS and is reported as the triplicate mean ± SD. The charts capture independently evolved isolates within the five lineages shown in Fig. 1B. D isolates are shown in orange and M isolates are shown in blue, and their respective colony morphologies are shown in Fig. S2. The numerical IDs correspond to Table S1, and mutations reflect the affected amino acid residues, except that frameshift (FS) and promoter region (PR) mutations refer to the specific nucleotides.

Loss-of-function mutations (i.e., nonsense and frameshift mutations) in *wspE* were exclusively associated with D to M transitions throughout all lineages to reduce c-di-GMP production (Table S1). These observations are not particularly surprising, since WspR cannot be phosphorylated in the absence of a functional WspE (Fig. 3). In contrast, multiple missense and in-frame deletions were observed in the phosphoreceiver domain of WspE to exclusively stimulate c-di-GMP production (Fig. 2). Accordingly, mutations within the conserved phosphoreceiver domain of CheY, a WspE homolog in *E. coli*, can activate the protein without phosphorylation (36, 37). In addition, the DGC activity of WspR in *P. aeruginosa* could be modulated in a phosphorylation-independent manner (18, 38). Artificial activation of WspE would deregulate WspA-dependent activation and was often the evolutionary solution to recover c-di-GMP production when the upstream signaling components of the Wsp system became functionally crippled (Table S1). The M isolate 1.4 of lineage 1 carries a frameshift mutation in *wspE*, which should terminally shut down the Wsp system, and the c-di-GMP level was reduced as predicted (Fig. 4). However, c-di-GMP production was restored in this lineage once again in the following D isolate 1.5 through a missense mutation in DgcH (V459G), a bioinformatically predicted DGC that impacts biofilm formation in *P. aeruginosa* PAO1 (39). DgcH is capable not only of producing c-di-GMP, but of producing it at one of the highest levels detected in our study (Fig. 4, Table S1). In contrast to the Wsp system, it is difficult to predict functional consequences of mutations in other DGCs, since so little is known beyond their conserved catalytic domain.

Many DGCs are functionally capable of causing the M to D shift independently from WspR. Sequential patterns of mutations and c-di-GMP quantification across all 33 lineages indicate that the DGC DgcH is also a dominant contributor to the intracellular c-di-GMP pool under our experimental conditions. Other known or predicted DGCs were typically targeted to modulate c-di-GMP levels after the Wsp system and DgcH became genetically dysfunctional. One exception is MorA, which represents the first mutation target in two lineages (Table S1). The first D isolate 4.1 of lineage 4 carries an in-frame deletion mutation in *dgcH* that removes amino acid residues 524 to 537 (Fig. 4 and 5). Interestingly, the

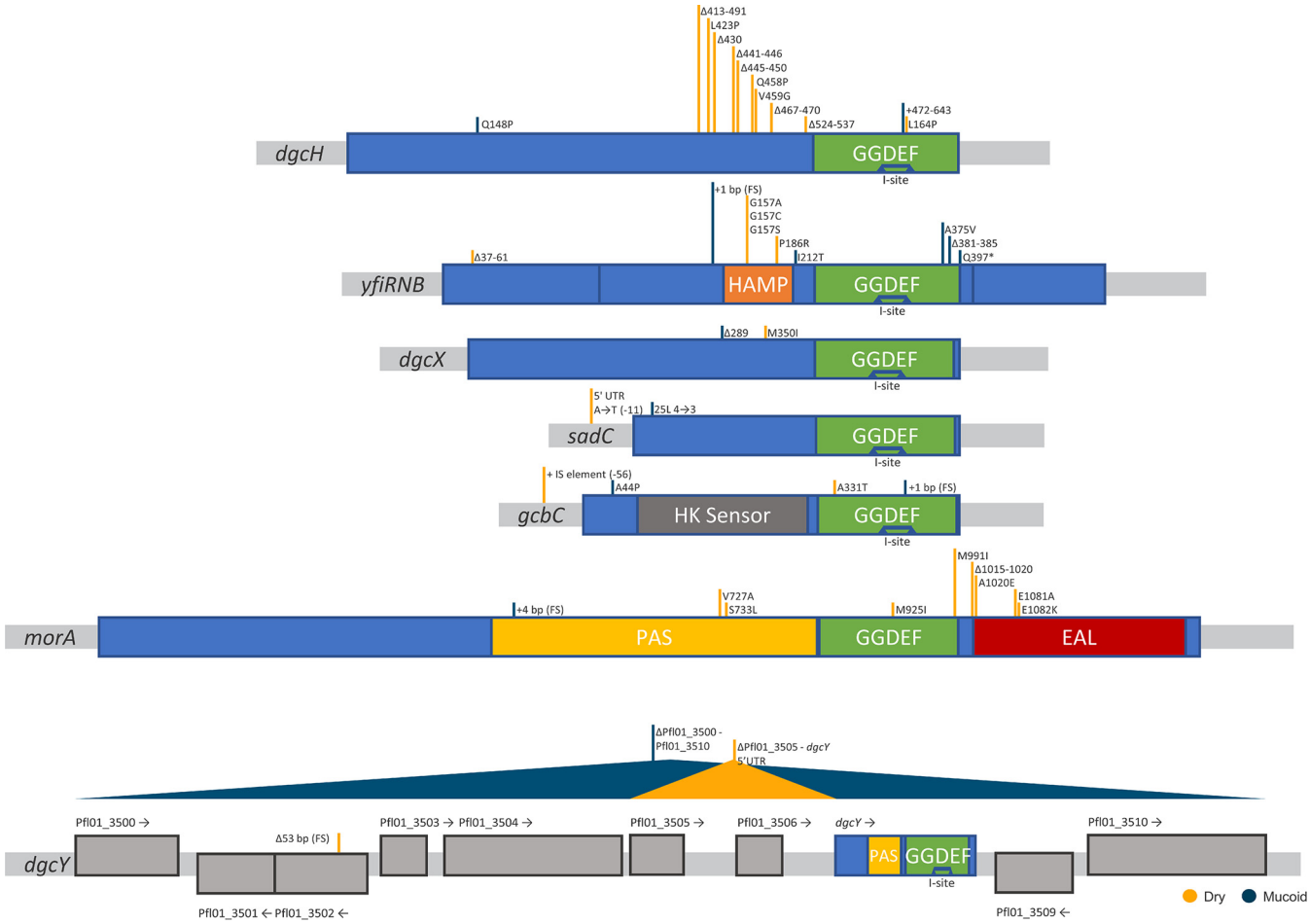

FIG 5 Alignment of our mutation data to annotated domains in known or predicted DGCs. Blue boxes represent the protein sequence, and their flanking gray boxes represent untranslated regions. Each image represents a single DGC as indicated, with the exception of *yfiRNB* and *dgcY*. *YfiRNB* shows three blue boxes, with each box representing YfiR, YfiN (DGC), or YfiB, respectively. *DgcY* shows a cluster of 10 genes with 9 hypothetical genes of undetermined function and 1 bioinformatically predicted DGC (*dgcY*). Domain data were derived from CDD (NCBI): GGDEF, c-di-GMP catalytic domain; PAS, sensory signaling domain, EAL, phosphodiesterase hydrolysis domain; HAMP, transmembrane relay domain; I-site, c-di-GMP allosteric regulation site (shown inside GGDEF); HK sensor, histidine kinase sensory domain. Mutations that stimulate c-di-GMP production are indicated by orange horizontal bars, and those that reduce c-di-GMP production are indicated by blue horizontal bars.

GGDEF diguanylate cyclase domain of DgcH spans residues 537 to 693, and the removal of the immediately adjacent residues appears to activate c-di-GMP production. We observed a reduction in c-di-GMP in the following M isolate 4.2, which has a missense mutation in DgcH (L634P). A search against NCBI's conserved domain database identifies that residues 619 to 643 contain the inhibitory I-site (24, 40), with residue N637 as the predicted interaction site with c-di-GMP. Our sequence analysis supports this annotation and the likelihood that DgcH is under allosteric control by c-di-GMP; the L634P mutation in DgcH could mimic a c-di-GMP bound state to cause the observed reduction in c-di-GMP. We cannot discount the possibility of additional regulatory mechanisms, since numerous missense and in-frame deletion mutations were detected across the coding sequence of DgcH (Fig. 5). As already discussed above, the V459G mutation in DgcH greatly increased c-di-GMP production in lineage 1 (Fig. 4), and in lineage 27, the Q454P mutation caused a shift to the D phenotype and then reverted back to the M phenotype through another missense mutation (Q148P) (Table S1). Similar to DgcH, specific missense mutations in other DGCs caused bidirectional shifts, and most activating mutations were found outside their conserved catalytic domain (Fig. 5). We also detected the I-site in other DGCs, with MorA being the lone exception, but no associated mutations were observed (Fig. 5). To the best of our knowledge, no functional studies have been carried out to characterize the bioinformatically predicted domains of these DGCs beyond their catalytic domain. We have clearly established that mutations

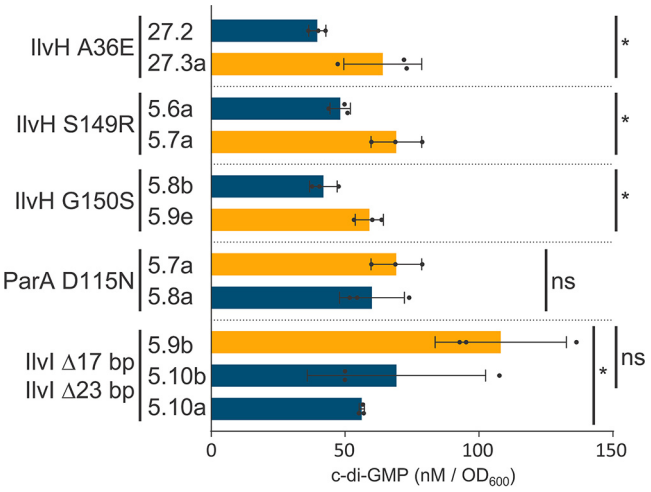

FIG 6 C-di-GMP levels fluctuate with mutations in genes with BCAA biosynthesis function. C-di-GMP measurements are triplicate mean ± SD. Raw c-di-GMP values of each mutant and its respective parent are reported in Table S1. The causal mutation of each phenotypic shift is indicated on the left. D isolates are shown in orange, and M isolates are shown in blue. (Student's *t* test: ns, nonsignificant; *, $P < 0.05$).

observed in this study impact c-di-GMP production, which should stimulate future studies to characterize their catalytic and/or regulatory consequences.

Mutations in genes with previously unknown associations with c-di-GMP production integrate with Wsp or other DGC mutations to modulate c-di-GMP levels. We also observed mutations in bioinformatically annotated genes with no known associations to c-di-GMP modulation but with clear associations with Wsp components and other DGCs. This pattern is best represented in lineage 5 (Fig. 4). Like most lineages, mutations initially accumulate within *wsp* genes and deregulate the Wsp system. Subsequent isolates D 5.5 and M 5.6 carry mutations that activate and then deactivate the DGC SadC, respectively. Surprisingly, isolate 5.7 returns this lineage to the D phenotype through a missense mutation in IlvH (G150S), which is predicted to function in the biosynthesis of branched-chain amino acids (BCAA). We observed three independent missense mutations in IlvH across our study that exclusively cause a phenotypic shift from M to D and reduced motility (Table S1). Accordingly, quantification of c-di-GMP shows that each of these three mutations significantly increases c-di-GMP respective to their immediate M parent (Fig. 6). These results indicate that a previously unknown relationship exists between BCAA biosynthesis and c-di-GMP production, and we explore this relationship in detail below.

Lineage 5 returns to the M phenotype in isolate 5.8 through a missense mutation in the hypothetical protein Pfl01_0730 (D115N) (Fig. 4). This protein, here ParA (PAP2 associated c-di-GMP regulator), shares homology with the PAP2 superfamily of proteins, suggesting that it may be involved in phospholipid turnover and impact the bioavailability of phosphate within the cell (41). Although we found the relative decrease in c-di-GMP in isolate 5.8 to be not statistically significant from its parent likely due to technical noise (Fig. 6), the observed mutation clearly drives the phenotypic transition from D to M. Furthermore, if this mutation does not impact c-di-GMP levels, then we would not expect a further transition through elevated c-di-GMP production. Indeed, we captured two independent transitions back to the D phenotype, both with substantially increased c-di-GMP levels (Fig. 4). Isolates 5.9a and 5.9b are sister isolates (i.e., they share a parent) that have developed unique chimeric Wsp proteins. Both chimeric proteins (WspA::D and WspB::D) contain identical partial segments of WspD commencing at residue 158, situated immediately adjacent to the in-frame deletion detected in their common ancestral isolate 5.4, which previously deactivated the Wsp system (Fig. 4). To determine whether these chimeric proteins alone are sufficient to drive the phenotypic shift from M to D, we replaced the corresponding native Wsp proteins in the ancestral M isolate with each chimeric protein. In parallel, we also replaced the corresponding naturally modified Wsp proteins in the immediate parental M isolate 5.8 with each chimeric protein. Both engineered isolates in the ancestral M background retained the M phenotype, but both engineered isolates in the M isolate 5.8 background recapitulated the D transition

TABLE 1 Reconstructing select naturally acquired mutations in both the ancestral and direct parent isolates reveals dependence on the previous mutation(s) to drive specific M-D phenotypic shifts

Isolate ID	Mutation	CDS ID[a]	Mutant phenotype	Parent isolate ID	Mutation in parent	Ancestor[b]	Reconstructed mutants[c]	
							Parent	Ancestor
5.9a	WspA::D	Pfl01_1052::1055	Dry	5.8a	ParA (D115N)	M	Dry	Mucoid
5.9b	WspB::D	Pfl01_1053::1055	Dry	5.8a	ParA (D115N)	M	Dry	Mucoid
30.1	WspC::D	Pfl01_1054::1055	Dry	Δ*rsmE*	Δ*rsmE*	M	Dry	Dry
27.3b	IlvH (A36E)	Pfl01_4787	Dry	27.2	DgcH (Q148P)	M	Dry	Mucoid
5.7a	IlvH (S149R)	Pfl01_4787	Dry	5.6a	SadC (25L 4→3)	M	Dry	Mucoid
5.9e	IlvH (G150S)	Pfl01_4787	Dry	5.8b	YfiN (I212T)	M	Dry	Mucoid
5.10b	IlvI (Δ17 bp)	Pfl01_4788	Mucoid	5.9b	WspB::D	D	Mucoid	Dry
5.10a	IlvI (Δ23 bp)	Pfl01_4788	Mucoid	5.9b	WspB::D	D	Mucoid	Dry
6.5a	DgcY (Δ3505-3506)	Pfl01_3505-3506	Dry	6.4	WspE (+1bp)	M	Dry	Mucoid
6.6a	DgcY (Δ3500-3510)	Pfl01_3500-3510	Mucoid	6.5a	DgcY (Δ3505-3506)	D	Mucoid	Dry
2.3	NarA (A383S)	Pfl01_3147	Dry	2.2	WspD (W90L)	M	Dry	Mucoid
10.2	CalM (+5 bp)	Pfl01_1895	Mucoid	10.1	DgcH (Δ467-470)	D	Mucoid	Dry
11.2	RndA (Q51S)	Pfl01_2749	Mucoid	11.1	WspA (A381V)	D	Mucoid	Dry
6.8a	CdrB (A290T)	Pfl01_0652	Mucoid	6.7c	YfiN (G157C)	D	Mucoid	Dry

[a]CDS, coding DNA sequence.
[b]Ancestors are the reference M or D isolates (Fig. 1).
[c]Each mutation was reconstructed in the direct parent and the corresponding ancestor isolate. WGS confirmed the reconstruction of each mutation.

that was observed in isolates 5.9a and 5.9b (Table 1). These results indicate that the two chimeric Wsp proteins require additional mutation(s) observed within this lineage to produce c-di-GMP. Both the WspA::D and WspB::D chimeras have lost WspC, which is not surprising since the methylation sites of WspA were removed previously in the D isolate 5.3. Similarly, WspB is completely removed in the WspA::D chimera, and nearly 75% of WspB has been removed in the WspB::D chimera. At this stage, it remains unclear whether the observed mutations in *ilvH* and/or *parA* are required for the function of the two Wsp chimeras. However, we present additional evidence below that strengthens the relationship between IlvH and the Wsp system.

The WspB::D chimera isolate 5.9b was next used to evolve M progeny isolates. Sister isolates 5.10a and 5.10b were each found to carry frameshift deletions in *ilvI* that decreased c-di-GMP levels (Fig. 4). The two *ilvI* mutants carry a deletion of 17 or 23 nucleotides that start at the same position, which should abolish IlvI's function by causing a frameshift. IlvI and IlvH form a complex that catalyzes the first step of BCAA biosynthesis, where IlvH serves as the regulatory subunit and IlvI serves as the catalytic subunit (42). IlvH in *E. coli* has been bioinformatically predicted to respond to c-di-GMP levels due to the presence of the inhibitory I-site (40), which we also detected in most DGCs (Fig. 5). We identified that IlvH of *P. fluorescens* Pf0-1 also contains the I-site RXXD motif at residues 103 to 106. None of the independently identified IlvH mutations (A36E, S149R, and G150S) in our study fall within this motif, but all three mutations significantly increase c-di-GMP levels (Fig. 6). All identified mutations in IlvH fell outside the core RXXD motif. However, it does not necessarily mean these are not the key residues contributing to the binding affinity of c-di-GMP. Beyond the potential allosteric regulation of IlvH by c-di-GMP, there is no known relationship between BCAA biosynthesis and c-di-GMP production to the best of our knowledge. However, we subsequently observed frameshift mutations in the catalytic subunit (IlvI) that return this lineage back to the M phenotype with reduced c-di-GMP levels.

The frameshift mutations in *ilvI* should lead to BCAA auxotrophy, which is likely masked by the nutrient-rich medium utilized in our experimental evolution system. To test this prediction, we grew isolates 5.10a and 5.10b in a chemically defined minimal medium without BCAA. We did not observe any growth unless BCAA was exogenously supplemented (Fig. S3), confirming that our *ilvI* mutants are unable to synthesize BCAA. We next tested if exogenous supplementation of BCAA alone could restore c-di-GMP production in the *ilvI* mutant (M isolate 5.10a). Since the *ilvI* mutant cannot grow in the minimal medium without BCAA supplementation, we also included our M and D ancestors (Fig. 1A) as relative controls in addition to the *ilvH* mutant (D isolate 5.7) and the *parA* mutant (M isolate 5.8) from the same lineage. Exogenous

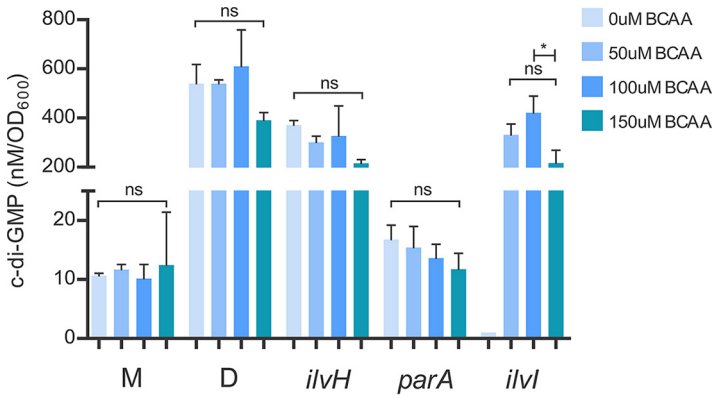

FIG 7 BCAA supplementation stimulates c-di-GMP production in a BCAA auxotroph with the M phenotype but does not impact c-di-GMP production in non-BCAA auxotrophs with the same M phenotype. Isolates were grown in the chemically defined PMM medium with 0, 50, 100, or 150 μM BCAA supplementation (valine, leucine, isoleucine). C-di-GMP was extracted and quantified via LC-MS/MS in triplicate and plotted as the mean with STD (ANOVA; Tukey's honestly significant difference [HSD] posttest: ns, nonsignificant; *, $P < 0.05$). M and D refer to the ancestral M and D isolates in Fig. 1A. The *ilvH* mutant (D isolate 5.7) produces c-di-GMP levels similar to those of the D isolate control, and the *parA* mutant (M isolate 5.8) produces c-di-GMP levels similar to the M isolate control. These relative patterns are consistent with the c-di-GMP quantification data reported in Fig. 6 under nutrient-rich conditions. Exogenous supplementation of BCAA across all concentrations does not significantly impact c-di-GMP production. There are no data for the *ilvI* mutant at 0 μM BCAA, since this isolate fails to grow in PMM unless BCAA is exogenously provided. However, the *ilvI* mutant (M isolate 5.10a) produces c-di-GMP levels comparable to those of both D and the *ilvH* mutant (D isolate 5.7) with BCAA supplementation.

supplementation of BCAA in the *ilvI* mutant indeed restored c-di-GMP production at comparable levels to both D and the *ilvH* mutant (D isolate 5.7) (Fig. 7). In contrast, c-di-GMP levels remained the same in both M and the *parA* mutant (M isolate 5.8) whether or not BCAA was added (Fig. 7). These results show that exogenous supplementation of BCAA does not correlate with c-di-GMP production, at least across the concentration range we have tested (50 to 150 μM). We chose this range for our experiment since higher concentrations did not impact the growth of either the ancestral M or the *ilvI* mutants in the minimal medium (Fig. S3). Given that there is no evidence of exogenous BCAA dose dependence on c-di-GMP production across all tested strains of either the M or D phenotype (Fig. 7), it is unlikely that higher concentrations of BCAA will amplify c-di-GMP production. Although BCAA supplementation restores c-di-GMP production in the *ilvI* mutant in the minimal medium, the reduction of c-di-GMP levels observed in the same *ilvI* mutant under our nutrient-rich experimental evolution conditions (Fig. 6) is not likely associated with losing the ability to synthesize BCAA. Accordingly, reconstructing the two frameshift *ilvI* mutations independently in the ancestral D isolate did not cause a shift to the M phenotype, but the initially observed shift to the M phenotype was recapitulated when these mutations were introduced into their direct parental D isolates (Table 1). Since IlvI forms a complex with IlvH, the observed frameshift mutations in *ilvI* likely decouple the complex and consequently impact IlvH's function to modulate c-di-GMP production. Lineage 5 returns to the D phenotype in four sister branches following the *ilvI* mutations through mutations in *wspE* or *dgcH* (Fig. 4). As already discussed above, we commonly observed activating *wspE* mutations when the upstream signaling Wsp components are disrupted, and the in-frame deletion in *dgcH* is also identical to the deletion reported in the D isolate 4.1. These four independent transition steps into the D phenotype clearly indicate that the catalytic activity of IlvI is not required for c-di-GMP production.

Lineage 27 was commenced with an engineered Δ*wspCD* M isolate (Table S1, isolate 27.0), where we also observed the shift to the D phenotype through a missense mutation in IlvH (A36E) by restoring c-di-GMP production (Fig. 6). In contrast to the M-shifting ParA (D115N) mutation that followed the D-shifting IlvH (G150S) mutation in lineage 5, the transition from IlvH (A36E) to the M phenotype was associated with a mutation which converts the stop codon of *wspB* with a cysteine residue to extend its open reading frame, but out of frame with *wspE* (both *wspC* and *wspD* were already deleted). A common trend exists

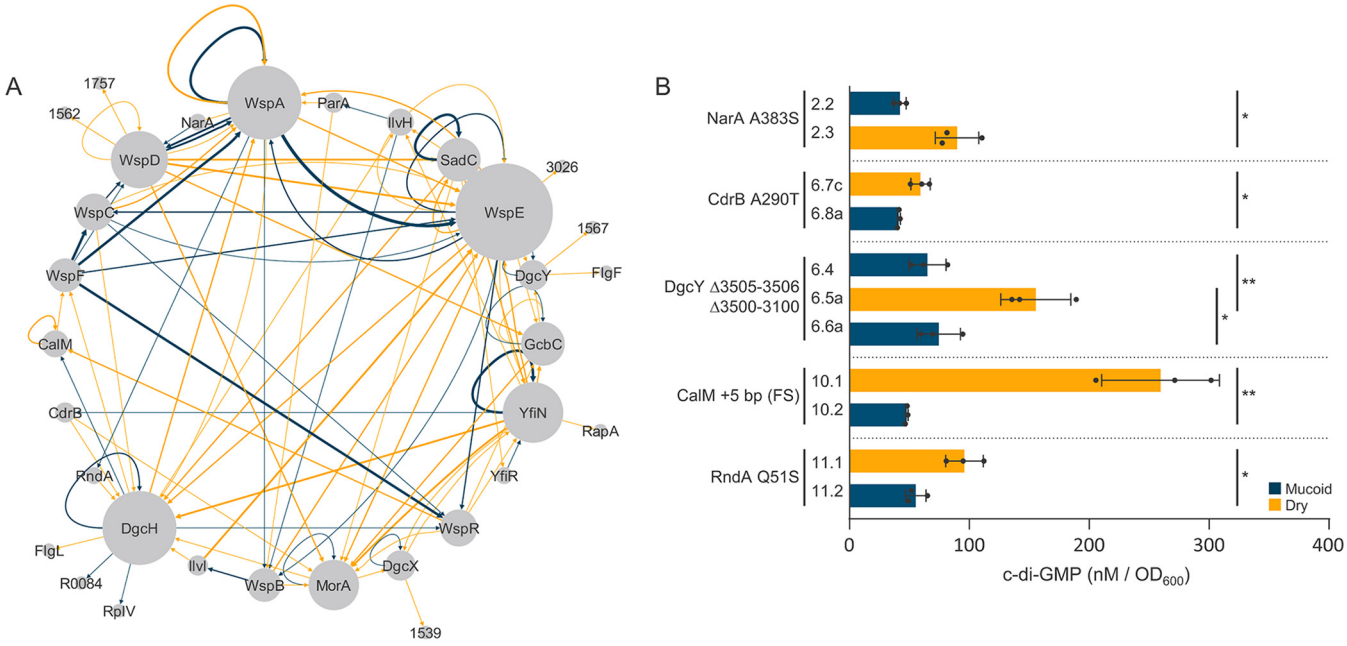

FIG 8 A node-edge representation of 147 unique mutations across 33 lineages and c-di-GMP quantification data of isolates with mutations in proteins with significant network connectivity that are not known to be associated with c-di-GMP modulation. (A) A node-edge plot reveals focal proteins under selection. Each node represents a protein, and each edge represents a relationship where one mutation precedes or proceeds another. Orange edges represent M to D shifts, and blue edges represent D to M shifts. The relative size of a node and thickness of an edge is proportional to frequencies within the data set. Proteins that collectively form the ring represent commonly mutated targets in this study and likely have a substantial role in c-di-GMP regulation. Proteins with limited connectivity fall outside the main ring. (B) LC-MS/MS validates that proteins with significant network connectivity, but not previously associated with c-di-GMP, have a significant impact on intracellular c-di-GMP levels. C-di-GMP measurements are reported as the triplicate mean ± SD. C-di-GMP values of each mutant and its respective parent are summarized in Table S1 with the corresponding ID tag. D isolates are shown in orange, and M isolates are shown in blue. (Student's *t* test: *, $P < 0.05$; **, $P < 0.01$).

between lineages 5 (Fig. 4) and 27 (Table S1) in that multiple mutations first occur in Wsp proteins, which are proceeded by mutations in a non-Wsp DGC (SadC or DgcH respectively), and then unique missense mutations occur in IlvH to stimulate c-di-GMP production. Reconstructing the three IlvH missense mutations in the ancestral M isolate does not lead to a shift to the D phenotype, but reconstructing these mutations in their direct parental M isolate recapitulates the initially observed shift to the D phenotype (Table 1). The common targets of mutations between the two lineages that converge on IlvH mutations are Wsp proteins, which implies that the c-di-GMP-stimulating mutations in IlvH specifically associate with a deregulated Wsp system. Furthermore, the undoing of the IlvH (A36E)-induced c-di-GMP production by the stop codon mutation in *wspB* implies potential IlvH-Wsp interactions that are unlikely to be purely metabolic in nature.

A macro assessment of sequential mutation patterns across all 33 parallel lineages captures potential associations within the c-di-GMP regulome. A long-standing question in the field is why microbes possess so many independent DGC and/or PDE machineries. A systematic analysis of genes that are bioinformatically predicted to be DGCs in *P. fluorescens* demonstrated that most have little impact on the intracellular c-di-GMP pool (9), and a significant number of DGCs/PDEs in *E. coli* are present in an inactive form (8). In addition, independent DGCs could regulate a subcellularly localized role (11) that could also contribute to the total intracellular pool to regulate diverse physiological pathways across a gradient (10). Our study indicates that many known or predicted DGCs could be independently stimulated to trigger a common phenotypic shift, which appears to operate across a broad range of c-di-GMP levels (Fig. 1C). We also captured mutations in genes with unknown associations with c-di-GMP modulation that significantly impact the c-di-GMP pool (Table S1). Repetitive patterns of sequential mutations across independently evolving lineages could reveal previously unknown connectivity between discrete regulatory and catalytic elements.

To visualize conserved patterns of mutations across our complex data set, we compiled all sequences of mutation events across the 33 parallel lineages into a single node-edge plot (43) (Fig. 8A). The nodes represent the mutated genes in our experiment. The edges (i.e., lines) of the plot report if the mutation causes an M (blue) or D (orange) phenotype, and the

thickness of the edge reflects the frequency of the observed pattern (Table S2). Proteins that are integrated into this plot—meaning that many edges connect to a specific node—collectively form the main ring. Nodes associated with a single edge fall out of this ring, and mutations in these proteins typically occur at the end of a lineage or a branched sublineage that was not sequenced. Since we did not sequence any progeny isolates from these 10 mutants that fall outside the main ring, we will not discuss them further.

The largest nodes in Fig. 8A are represented by Wsp proteins, DgcH, and other known DGCs such as YfiN, GcbC, MorA, and SadC. The majority of DGCs have blue recursive edges that cause an M phenotype, which indicates that mutations occur in the same protein to shut down its activity, immediately following a mutation that initially stimulated its activity. The high frequency of blue recursive edges associated with each DGC and yellow edges between distinct DGCs collectively indicates that each DGC simply replaces another to restore c-di-GMP production. Blue edges between DGCs are extremely rare, which suggests that individual DGCs do not directly interact with each other. Notably, there are several proteins with both yellow and blue edges that are integrated in this plot and have not been shown to have a role in c-di-GMP regulation or production. We next infer potential functions of these proteins with respect to c-di-GMP modulation.

NarA (*N*-ethylammeline chlorohydrolase-associated c-di-GMP regulator). Pfl01_3147 is annotated as a hypothetical protein, but we found homology to an *N*-ethylammeline chlorohydrolase. In isolate 2.3, we observe that the A383S mutation in NarA increases c-di-GMP levels (Fig. 8B), which confirms that this hypothetical protein is indeed biologically active. This NarA mutation follows the M-shifted W90L mutation in WspD, which suggests that NarA is either able to restore Wsp signaling or activate other DGCs to increase c-di-GMP levels. We have no reason to suspect that NarA directly catalyzes c-di-GMP, since it lacks any c-di-GMP-associated domains or motifs. The progeny of this NarA mutant carries a nonsense mutation in *wspD*, reverting this isolate back to an M phenotype (Table S1). Thus, the A383S mutation in NarA associates specifically with *wspD* mutations to both restore and shut down c-di-GMP production. *N*-ethylammeline is a derivative of ammeline, and a recent study theorized that ammeline is likely an essential building block required for the synthesis of cyclic complexes (44). Although the metabolic connections are unknown, there is a strong indication that NarA interacts with WspD at some capacity to modulate c-di-GMP levels.

CdrB. Pfl01_0652 encodes a protein that shares homology with the transporter protein CdrB in *P. aeruginosa* (PA4624) (45–47). In our lineage 6, the missense mutation YfiN (G157C) increases c-di-GMP production, which is immediately followed by the CdrB A290T missense mutation to decrease c-di-GMP levels (Fig. 8B). This suggests that an unaltered CdrB or its native transport activity is necessary for YfiN's DGC activity. Mutations that follow the CdrB mutation occur in *morA* or *dgcH*, each increasing c-di-GMP as indicated by the D-phenotype (Table S1). Therefore, the negative impact of our CdrB mutation on YfiN could be recovered through the genetic activation of other DGCs, which could also reflect interactions with CdrB. Expression of the *cdrB* gene increases proportionally with intracellular levels of c-di-GMP during biofilm formation (47), but it has no identified role in c-di-GMP modulation.

CalM (c-di-GMP-associated LysM). The hypothetical gene Pfl01_1895, here *calM*, is a commonly mutated gene in our study (Table S1). We observed a duplication of five nucleotides within *calM* that results in a significant decrease in c-di-GMP (Fig. 8B). Two repetitive clusters of CAGCG shift to three clusters to cause a frameshift. This mutation follows a *dgcH* in-frame deletion that dramatically increases c-di-GMP production, indicating that CalM impacts DgcH's activity. Remarkably, three independently evolved progeny isolates in this lineage carry mutations that remove the initial five-nucleotide insertion, returning each isolate back to the D phenotype, likely by restoring DgcH's activity (Table S1). CalM contains domains with homology to the LysM peptidoglycan-binding superfamily and the FimV C-terminal transmembrane domain that is implicated in modulating motility (48, 49). The presence of such domains suggests a potential link to peptidoglycan stress, and peptidoglycan stress has been associated with surface-sensing through the Wsp system in *P. aeruginosa* (33).

RndA (RND transporter). Pfl01_2749 is bioinformatically predicted to encode an RND transporter, which functions as an efflux pump to remove toxins, antibiotics, quorum

sensing molecules, and other metabolites (50). We observed that the nonsense mutation Q51* in *rndA* significantly decreases c-di-GMP levels (isolate 11.2, Fig. 8B). The *rndA* mutant then shifts to the D phenotype through an in-frame deletion that removes amino acid residues 524 to 537 in DgcH. This specific mutation was observed in multiple lineages to exclusively stimulate c-di-GMP production. Interestingly, a recent study speculates that quorum sensing molecules could contribute to a feedback loop to inhibit c-di-GMP production (51).

DgcX and DgcY (bioinformatically predicted DGCs). Pfl01_3550 and Pfl01_3508 are both bioinformatically predicted to encode DGCs, but their enzymatic function has not yet been demonstrated. Here, we establish that they are both functionally active in c-di-GMP catalysis and annotate them as *dgcX* and *dgcY*, respectively, since genes *dgcA* through *dgcW* already exist. Pfl01_3550, here *dgcX*, is a commonly mutated gene in our data set which increases c-di-GMP (Table S1). We observed a blue recursive loop in the node-edge plot for DgcX, which is consistent with other known DGCs (Fig. 8A). We isolated two independently evolved D mutants with the same M350I mutation and an M mutant with an in-frame deletion of L289. Phenotypic and motility data support that the observed mutations in *dgcX* influence the intracellular c-di-GMP pool. The genomic location of *dgcY* is in a region of hypothetical genes that appear to form an operon. Interestingly, our *dgcY* mutants carry large deletions of the hypothetical genes within this genomic region (Fig. 5). The deletion of Pfl01_3505, Pfl01_3506, and the 5′ untranslated region (UTR) region of *dgcY* results in a significant increase in c-di-GMP (isolate 6.5a, Fig. 8B), which likely replaces the native promoter region of *dgcY* with that of Pfl01_3505. C-di-GMP is significantly decreased in the progeny isolate 6.6a (Fig. 8B) after the deletion of Pfl01_3500-Pfl01_3510, which includes *dgcY*. It is unclear whether the encoded proteins of the hypothetical genes that flank *dgcY* are functionally related to DgcY. We had initially suspected that these hypothetical genes could encode a complex signal transduction system like Wsp, but we did not detect any homologous Wsp domains or other c-di-GMP-associated motifs.

To confirm whether the observed mutations in these atypical c-di-GMP-associated genes alone could modulate c-di-GMP levels, we reconstructed representative mutations in their respective ancestral backgrounds. None of the engineered isolates produced a phenotypic shift, but reconstructing the same mutations in their direct parental isolates recapitulated the initially observed phenotypic shifts (Table 1). These results clearly indicate that specific mutations in the associated DGCs are first required to impact c-di-GMP levels. Although functional studies are required to prescribe specific mechanisms, diverse cellular processes appear to be integrated with numerous catalytic machineries to modulate the c-di-GMP pool in *P. fluorescens*, and the missense and in-frame deletion mutations observed in Wsp proteins and other DGCs (Fig. 5) could reflect potential interaction sites.

Conclusion. Although we have extensive knowledge of how specific enzymes make or break c-di-GMP and how this molecule interacts with a large number of regulatory elements to modulate diverse physiological processes, relatively little is known about how C-di-GMP production itself is regulated. This study takes advantage of a repeatedly evolving social behavior in *P. fluorescens* to demonstrate how numerous proteins could independently and collectively produce remarkable sequences of genetic innovation to regulate c-di-GMP levels. Our extensive library of functionally critical residues reinforces the current model of the Wsp system, which heavily draws functional analogies to the *E. coli* chemotaxis system and particularly lacks domain resolution in WspB and WspD. Beyond the Wsp system, we have confirmed that several bioinformatically predicted DGCs are indeed enzymatically active and identified unique missense and in-frame deletion mutations in multiple DGCs that fall outside their conserved catalytic domain. These mutations likely reflect regulatory domains that are critical for modulating enzymatic activity. We have also uncovered a set of unexpected or hypothetical proteins that clearly have the capacity to influence c-di-GMP turnover. Three missense mutations in *ilvH* were identified to independently stimulate c-di-GMP production, which appears to be independent of IlvH's primary role in BCAA biosynthesis but, rather, operates through an unknown interaction with the Wsp system. We have identified the same I-site in IlvH as in most DGCs, which suggests that IlvH physically interacts with c-di-GMP. Similarly, CdrB and RndA homologs in other organisms have been implicated to respond

to c-di-GMP levels, but they have never been associated with modulating c-di-GMP production. We have confirmed that the mutations observed in these proteins alone do not impact c-di-GMP levels but do so specifically in the presence of genetically modified DGCS or the Wsp signal transduction system.

An emerging concept here is that the intracellular pool of c-di-GMP, whether it be subcellularly localized or in sum, appears to be modulated through the catalytic activities of many independent DGCs that are in tune with diverse proteins. Such intricacies are masked by the activities of DGCs with high output, but they are clearly hardwired in the genome of *P. fluorescens* and reflect a complex and underappreciated interconnectivity. Similar relationships could also manifest in other *Pseudomonas* and related species that share the same DGCs and unexpected proteins described in this study. In particular, very little is known about the functional domains of most DGCs beyond their conserved catalytic domain. The vast majority of the missense mutations or in-frame deletions captured in this study occur outside the catalytic domain to clearly activate or shut down c-di-GMP production. Our extensive library of functionally important mutations presented here should facilitate mechanistic studies of phylogenetically conserved DGCs that remain heavily underexplored.

MATERIALS AND METHODS

Strains and culture conditions. All *Pseudomonas fluorescens* Pf0-1 (52) isolates associated with parallel experimental evolution are described in Table S1, and engineered isolates are described in Table 1. Cells were routinely grown in Lennox LB (Fisher BioReagents) or *Pseudomonas* minimal medium (PMM) (53) or on *Pseudomonas* agar F (PAF) (Difco). *Pseudomonas* F (PF) broth (a nonagar variant of PAF) was prepared with the following ingredients: pancreatic digest of casein, 10 g/L (Remel); proteose peptone no. 3, 10 g/L (Remel); dipotassium phosphate, 1.5 g/L (Sigma-Aldrich); and magnesium sulfate, 1.5 g/L (Sigma-Aldrich). Cultures were incubated at 30°C and shaken at 250 rpm when applicable.

Parallel experimental evolution. Pure cultures of the ancestral M isolate or engineered M isolates were grown overnight in 5 mL LB broth, and 25-μL volumes were spotted on PAF plates and then incubated at room temperature for 3 to 8 days to allow spreading fans to emerge. To ensure consistency across experiments, PAF plates were always prepared and left to dry at room temperature for 2 days before being inoculated. One fan was randomly sampled from each colony and streaked on LB plates in duplicate. Sampling a fan always produced two isolates with either a mucoid (M) or dry (D) colony phenotype. A single isolated colony exhibiting the D phenotype was randomly chosen to start a new liquid culture and was also frozen down. This process was repeated to sample six independent fans (i.e., six lineages). Three of the six independent D isolates were randomly chosen and cultured as described above to start the next round of experimental evolution. We repeated the same sampling process as above except that new M phenotypes were isolated instead. We bidirectionally selected M and D phenotypes for as many as 13 rounds for a single lineage, but the number of sampled fans at each step was reduced over time in a varying manner across independent lineages. In total, approximately 600 independently evolved isolates were frozen down across 33 parallel lineages. Every isolate was subjected to a motility assay in an LB plate with 0.25% agar, and the M and D ancestors were used as controls (29). In addition, 25 μL of pure culture of each isolate, the ancestral isolate with the opposite phenotype, and a 1:1 mixture of both were spotted onto PAF plates in triplicate and assessed for cooperative radial spreading (Fig. 1A) to filter out hypermotile and noncooperative mutants (29). Colony diameters were measured and recorded after 4 days of incubation at room temperature and considered cooperative if the measured diameter of the 1:1 colony exceeded the diameters of both the mutant and the respective ancestral isolate. Isolates that failed this test were removed from the study.

Reconstruction of naturally derived mutations in ancestral and direct parental backgrounds. Experimentally evolved isolates were whole-genome sequenced to identify the causal mutations as described below. We reconstructed select naturally acquired mutations in the respective ancestral background and also in the direct parental background using previously described methods (29). PCR primers were developed from the sequence data to amplify mutations of interest and are reported in Table S3. Isolates were grown overnight and underwent DNA extractions (Qiagen). Dream *Taq* DNA polymerase (Thermo Fisher) was used in PCRs with purified DNA to generate insert fragments carrying the mutations, which ranged in size from 456 bp to 934 bp. PCR was carried out using the recommended conditions of the Dream *Taq* amplification kit for amplicons below 2,000 bp. Inserts were cloned into the pGEM-T Easy vector system (Promega) and then subcloned into the NotI site of the suicide plasmid pSR47s (54). Suicide plasmids were heat-shocked into *E. coli* S17.1λ*pir*, mated with the target isolates reported in Table S3 on LB plates at 30°C for 16 h, and then plated onto PMM plates supplemented with 50 μg/mL kanamycin. We observed that *ilvI* mutants could not grow on PMM and therefore replaced the PMM selection plate with an LB plate supplemented with 50 μg/mL kanamycin and 100 μg/mL ampicillin for *ilvI* mutant constructs. Isolated colonies were grown overnight, serially diluted, and plated out on LB plates supplemented with 15% sucrose (wt/vol) for counterselection. Isolated colonies were placed in cryo-storage as described above. Crude DNA extracts were made for each isolate, where 100 μL of overnight culture was boiled at 100°C and centrifuged at 15,000 relative centrifugal force (RCF) for 30 s, and 10 μL of supernatant was used for PCR using the primers reported in Table S3. PCR

products underwent gel extraction and subsequent Sanger sequencing (primers in Table S3) to confirm that the mutation was successfully engineered into the target isolate. Upon PCR confirmation, pure cultures of cells from cryo-storage underwent DNA extraction (Qiagen) and were submitted for whole-genome sequencing (WGS), which confirmed that no additional mutations had accumulated in the target isolates during mutant construction.

DNA extraction, whole-genome sequencing, and variant calling. Pure cultures were grown overnight in 5 mL LB broth at 30°C. Then, 1 mL was spun down to form a pellet for DNA extraction. Pelleted cells were mechanically lysed with the Qiagen TissueLyser LT at 50 oscillations/s for 10 min. The Qiagen DNeasy UltraClean microbial DNA extraction kit was used following the standard operating procedures. Samples were then eluted into 30 μL H_2O after a 5-min incubation at 4°C with the elution medium and stored at −20°C prior to shipment. Genomic DNA library preparations were carried out by the Microbial Genome Sequencing Center (Pittsburgh, PA) following standard operating procedures. Pooled and indexed samples were sequenced on the NextSeq 2000 platform with 150-bp paired-end reads and were demultiplexed prior to data delivery. The Trimmomatic algorithm was used to group and quality filter paired reads at a Phred score of 20 using a 4-bp sliding window. The BreSeq algorithm was used to align the paired reads to the *P. fluorescens* Pf0-1 reference genome (CP000094.2) and evaluate for single nucleotide polymorphisms (SNPs), insertions, deletions, or rearrangements with a set minimum of 20× coverage. Output sequence data from BreSeq was manually evaluated for each isolate to determine the order of mutations for a given lineage, where each M mutation was inferred by a common mutation found between its two sister progeny D isolates.

Alignment of mutation data to annotated domains. Domain analyses of Wsp proteins and DGCs were conducted and rendered as previously described (19). Peptide sequences of the predicted or known DGCs were obtained from the *Pseudomonas* Genome Database (55). NCBI's Conserved Domain Database (CDD) was used to evaluate the functional domains (56). Mutation data of Wsp proteins from this study were manually mapped to the rendered consensus sequence of the respective Wsp protein (19).

C-di-GMP extraction and LC-MS/MS. A colony of each isolate was transferred to PF broth and grown overnight. Overnight cultures were diluted to an optical density at 600 nm (OD_{600}) of 0.04 in triplicate and incubated for 2 to 4 h until the samples reached an OD_{600} of 0.5 and then promptly processed for c-di-GMP extraction. We verified by microscopy that there was no clumping of cells at the time of c-di-GMP extraction. C-di-GMP extraction and quantification procedures followed the protocols established by the Michigan State University Research Technology Support Facility (MSU-RTSF): MSU_MSMC_009 protocol for di-nucleotide extractions and MSU_MSMC_009a for LC-MS/MS, with the following modifications. All the steps of c-di-GMP extraction were carried out at 4°C unless noted otherwise. A sample of 1 mL of 0.5 OD_{600} culture was centrifuged at 15,000 RCF for 30 s, and cell pellets were resuspended in 100 μL of ice-cold acetonitrile/methanol/water (40:40:20 [vol/vol/vol]) extraction buffer supplemented with a final concentration of 0.01% formic acid and 25 nM c-di-GMP-fluorinated internal standard (InvivoGen catalog [cat. no.] 1334145-18-4). Pelleted cells were mechanically disturbed with the Qiagen TissueLyser LT at 50 oscillations/s for 2 min. Resuspended slurries were incubated at −20°C for 20 min and pelleted at 15,000 RCF for 15 min at 4°C. The supernatant was transferred to a prechilled tube and then supplemented with 4 μL of 15% wt/vol ammonium bicarbonate (Sigma-Aldrich) buffer for stable cryo-storage. Extracts were stored at −80°C for less than 2 weeks prior to LC-MS/MS analysis at MSU-RTSF. Sample degradation was observed with repeated freeze-thaw cycles, so extracts were never thawed until LC-MS/MS analysis. All samples were evaporated under vacuum (SpeedVac, no heat) and redissolved in 100 μL mobile phase (10 mM tryptose blood agar [TBA]/15 mM acetic acid in water/methanol, 97:3 vol/vol, pH 5). LC-MS/MS quantification was carried out with the Waters Xevo TQ-S instrument with the following settings: c-di-GMP-F at *m/z* transition of 693 to 346 with cone voltage of 108 and collision voltage of 33; c-di-GMP at *m/z* transition of 689 to 344 with cone voltage of 83 and collision voltage of 31. C-di-GMP data were normalized to 25 nM c-di-GMP-F by MSU-RTSF to account for sample matrix effects and sample loss during preparation. OD_{600} measurements of the initial samples were used to report the quantified c-di-GMP as nM/OD and visualized with GraphPad Prism 9.

BCAA supplementation assay and c-di-GMP quantification. Pure cultures were grown overnight in 5 mL LB broth. Then, 5 μL of each culture was transferred into 5 mL PMM. Cultures were supplemented with the BCAA valine, leucine, and isoleucine as previously described (57). Assessment of growth with BCAA supplementation contained either 0 μM (loading control), 180 μM, 200 μM, 220 μM, 250 μM, or 300μM in triplicate. Samples were incubated at 30°C for 24 h with 250 rpm shaking. Cultures were manually pipetted to resuspend cells, and 300 μL of culture was transferred to a 96-well black-wall clear-bottom plate for OD_{600} quantification. OD was quantified using the SpectraMax plate reader, and background (determined from blanks) was removed from each quantified sample. Data analysis and visualization of growth during BCAA supplementation were conducted in Excel. To evaluate the relationship between BCAA and c-di-GMP, pure cultures were grown for 24 h at 30°C with 250 rpm shaking in PMM liquid medium containing either 0 μM, 50 μM, 100 μM, or 150 μM of supplemented BCAAs. OD_{600} measurements were taken and samples were diluted to an OD_{600} of 0.04 in PMM at the same BCAA concentrations. Samples were incubated for 24 h under the same conditions stated and then sonicated (time 0.00:20, pulse 01 01, amplitude 20%) to disrupt cell aggregates. OD_{600} measurements occurred every hour until the OD_{600} was approximately equal to 0.25. C-di-GMP analyte extraction was carried out as stated above with the modification that 2-mL cultures were used for cell lysis. Quantified values of c-di-GMP are reported as nM/OD_{600} and were visualized with GraphPad Prism 9.

Node-edge analysis and visualization. The data reported in Table S1 were used to generate the "to-from" table, which assesses mutation patterns at the gene/protein level (43). Counts were determined by the frequency of the to-from patterns calculated from Table S1, where a mutation in a given gene/protein (to) occurred after a mutation in another gene/protein (from). This table was uploaded to Cytoscape to visualize the nodes (to genes/proteins) and edges (counts). Default renderings of the plot reported node centrality (commonly mutated targets) through coordinate placement on the graph. This

metric was converted to node size, with larger nodes representing more commonly mutated targets. Nodes were manually aligned for visual clarity, with nodes connected by two or more edges being placed in the main ring and nodes with a single edge being placed outside the ring.

Data availability. Raw sequence data of the evolved isolates from this study are accessible at NCBI's Sequence Read Archive under BioProject accession number PRJNA877395. The raw data from c-di-GMP measurements, BCAA-supplemented growth measurements, and BreSeq summaries of the evolved isolates are available at https://github.com/wook-kim-lab/cyclic-di-gmp-modulation.

SUPPLEMENTAL MATERIAL

Supplemental material is available online only.

FIG S1, EPS file, 1.8 MB.

FIG S2, EPS file, 2.3 MB.

FIG S3, EPS file, 1.5 MB.

TABLE S1, DOCX file, 0.1 MB.

TABLE S2, DOCX file, 0.02 MB.

TABLE S3, DOCX file, 0.01 MB.

ACKNOWLEDGMENTS

W.K. designed the study, C.K. performed the experiments, and C.K and W.K analyzed data and wrote the manuscript.

We thank RTSF (Michigan State University) for services and assistance with LC-MS/MS analyses and MiGS (Pittsburgh, PA) for providing genome sequencing.

This study was funded by the Charles Henry Leach II Fund 217032 (W.K.) and the Faculty Development Fund G1700030 (W.K.) awarded by Duquesne University.

REFERENCES

1. Römling U, Galperin MY, Gomelsky M. 2013. Cyclic di-GMP: the first 25 years of a universal bacterial second messenger. Microbiol Mol Biol Rev 77:1–52. https://doi.org/10.1128/MMBR.00043-12.
2. Valentini M, Filloux A. 2016. Biofilms and cyclic di-GMP (c-di-GMP) signaling: lessons from *Pseudomonas aeruginosa* and other bacteria. J Biol Chem 291:12547–12555. https://doi.org/10.1074/jbc.R115.711507.
3. Wolfe AJ, Visick KL. 2008. Get the message out: cyclic-Di-GMP regulates multiple levels of flagellum-based motility. J Bacteriol 190:463–475. https://doi.org/10.1128/JB.01418-07.
4. Jenal U, Reinders A, Lori C. 2017. Cyclic di-GMP: second messenger extraordinaire. Nat Rev Microbiol 15:271–284. https://doi.org/10.1038/nrmicro.2016.190.
5. Tamayo R. 2019. Cyclic diguanylate riboswitches control bacterial pathogenesis mechanisms. PLoS Pathog 15:e1007529. https://doi.org/10.1371/journal.ppat.1007529.
6. Dahlstrom KM, Giglio KM, Sondermann H, O'Toole GA. 2016. The inhibitory site of a diguanylate cyclase is a necessary element for interaction and signaling with an effector protein. J Bacteriol 198:1595–1603. https://doi.org/10.1128/JB.00090-16.
7. Simm R, Morr M, Kader A, Nimtz M, Römling U. 2004. GGDEF and EAL domains inversely regulate cyclic di-GMP levels and transition from sessility to motility. Mol Microbiol 53:1123–1134. https://doi.org/10.1111/j.1365-2958.2004.04206.x.
8. Hengge R, Galperin MY, Ghigo JM, Gomelsky M, Green J, Hughes KT, Jenal U, Landini P. 2016. Systematic nomenclature for GGDEF and EAL domain-containing cyclic di-GMP turnover proteins of *Escherichia coli*. J Bacteriol 198:7–11. https://doi.org/10.1128/JB.00424-15.
9. Newell PD, Yoshioka S, Hvorecny KL, Monds RD, O'Toole GA. 2011. Systematic analysis of diguanylate cyclases that promote biofilm formation by *Pseudomonas fluorescens* Pf0-1. J Bacteriol 193:4685–4698. https://doi.org/10.1128/JB.05483-11.
10. Yan J, Deforet M, Boyle KE, Rahman R, Liang R, Okegbe C, Dietrich LEP, Qiu W, Xavier JB. 2017. Bow-tie signaling in c-di-GMP: Machine learning in a simple biochemical network. PLoS Comput Biol 13:e1005677. https://doi.org/10.1371/journal.pcbi.1005677.
11. Massie JP, Reynolds EL, Koestler BJ, Cong J-P, Agostoni M, Waters CM. 2012. Quantification of high-specificity cyclic diguanylate signaling. Proc Natl Acad Sci U S A 109:12746–12751. https://doi.org/10.1073/pnas.1115663109.
12. Huertas-Rosales Ó, Romero M, Heeb S, Espinosa-Urgel M, Cámara M, Ramos-González MI. 2017. The *Pseudomonas putida* CsrA/RsmA homologues negatively affect c-di-GMP pools and biofilm formation through the GGDEF/EAL response regulator CfcR. Environ Microbiol 19:3551–3566. https://doi.org/10.1111/1462-2920.13848.
13. Merritt JH, Ha D-G, Cowles KN, Lu W, Morales DK, Rabinowitz J, Gitai Z, O'Toole GA. 2010. Specific control of *Pseudomonas aeruginosa* surface-associated behaviors by two c-di-GMP diguanylate cyclases. mBio 1:e00183-10. https://doi.org/10.1128/mBio.00183-10.
14. Ravichandran A, Ramachandran M, Suriyanarayanan T, Wong CC, Swarup S. 2015. Global regulator MorA affects virulence-associated protease secretion in *Pseudomonas aeruginosa* PAO1. PLoS One 10:e0123805. https://doi.org/10.1371/journal.pone.0123805.
15. Wassmann P, Chan C, Paul R, Beck A, Heerklotz H, Jenal U, Schirmer T. 2007. Structure of BeF_3^--modified response regulator PleD: implications for diguanylate cyclase activation, catalysis, and feedback inhibition. Structure 15:1155. https://doi.org/10.1016/j.str.2007.06.016.
16. Moscoso JA, Jaeger T, Valentini M, Hui K, Jenal U, Filloux A. 2014. The diguanylate cyclase SadC is a central player in Gac/Rsm-mediated biofilm formation in *Pseudomonas aeruginosa*. J Bacteriol 196:4081–4088. https://doi.org/10.1128/JB.01850-14.
17. Giardina G, Paiardini A, Fernicola S, Franceschini S, Rinaldo S, Stelitano V, Cutruzzolà F. 2013. Investigating the allosteric regulation of YfiN from *Pseudomonas aeruginosa*: Clues from the structure of the catalytic domain. PLoS One 8:e81324. https://doi.org/10.1371/journal.pone.0081324.
18. De N, Pirruccello M, Krasteva PV, Bae N, Raghavan RV, Sondermann H. 2008. Phosphorylation-independent regulation of the diguanylate cyclase WspR. PLoS Biol 6:e67. https://doi.org/10.1371/journal.pbio.0060067.
19. Kessler C, Mhatre E, Cooper V, Kim W. 2021. Evolutionary divergence of the Wsp signal transduction system in Beta- and Gammaproteobacteria. Appl Environ Microbiol 87:e01306-21. https://doi.org/10.1128/AEM.01306-21.
20. Mantoni F, Paiardini A, Brunotti P, D'Angelo C, Cervoni L, Paone A, Cappellacci L, Petrelli R, Ricciutelli M, Leoni L, Rampioni G, Arcovito A, Rinaldo S, Cutruzzolà F, Giardina G. 2018. Insights into the GTP-dependent allosteric control of c-di-GMP hydrolysis from the crystal structure of PA0575 protein from *Pseudomonas aeruginosa*. FEBS J 285:3815–3834. https://doi.org/10.1111/febs.14634.
21. Giacalone D, Smith TJ, Collins AJ, Sondermann H, Koziol LJ, O'Toole GA. 2018. Ligand-mediated biofilm formation via enhanced physical interaction between a diguanylate cyclase and its receptor. mBio 9:e01306-21. https://doi.org/10.1128/mBio.01254-18.

22. Christen B, Christen M, Paul R, Schmid F, Folcher M, Jenoe P, Meuwly M, Jenal U. 2006. Allosteric control of cyclic di-GMP signaling. J Biol Chem 281:32015–32024. https://doi.org/10.1016/S0021-9258(19)84115-7.
23. Chan C, Paul R, Samoray D, Amiot N, Giese B, Jenal U, Schirmer T. 2005. Structural basis for the activity and allosteric control of diguanylate cyclase. Acta Crystallogr A. https://doi.org/10.1107/s0108767305089993.
24. De N, Navarro MVAS, Raghavan RV, Sondermann H. 2009. Determinants for the activation and autoinhibition of the diguanylate cyclase response regulator WspR. J Mol Biol 393:619–633. https://doi.org/10.1016/j.jmb.2009.08.030.
25. Dahlstrom KM, Collins AJ, Doing G, Taroni JN, Gauvin TJ, Greene CS, Hogan DA, O'Toole GA. 2018. A multimodal strategy used by a large c-di-GMP network. J Bacteriol 200. https://doi.org/10.1128/JB.00703-17.
26. Traverse CC, Mayo-Smith LM, Poltak SR, Cooper VS. 2013. Tangled bank of experimentally evolved *Burkholderia* biofilms reflects selection during chronic infections. Proc Natl Acad Sci U S A 110:E250–E259. https://doi.org/10.1073/pnas.1207025110.
27. O'Rourke D, FitzGerald CE, Traverse CC, Cooper VS. 2015. There and back again: consequences of biofilm specialization under selection for dispersal. Front Genet 6:18. https://doi.org/10.3389/fgene.2015.00018.
28. Lind PA, Farr AD, Rainey PB. 2015. Experimental evolution reveals hidden diversity in evolutionary pathways. Elife 2015:e07074. https://doi.org/10.7554/eLife.07074.
29. Kim W, Levy SB, Foster KR. 2016. Rapid radiation in bacteria leads to a division of labour. Nat Commun 7:10508. https://doi.org/10.1038/ncomms10508.
30. Spiers AJ, Kahn SG, Bohannon J, Travisano M, Rainey PB. 2002. Adaptive divergence in experimental populations of *Pseudomonas fluorescens*. I. Genetic and phenotypic bases of wrinkly spreader fitness. Genetics 161:33–46. https://doi.org/10.1093/genetics/161.1.33.
31. Bantinaki E, Kassen R, Knight CG, Robinson Z, Spiers AJ, Rainey PB. 2007. Adaptive divergence in experimental populations of *Pseudomonas fluorescens*. III. Mutational origins of wrinkly spreader diversity. Genetics 176:441–453. https://doi.org/10.1534/genetics.106.069906.
32. Armbruster CR, Lee CK, Parker-Gilham J, de Anda J, Xia A, Zhao K, Murakami K, Tseng BS, Hoffman LR, Jin F, Harwood CS, Wong GC, Parsek MR. 2019. Heterogeneity in surface sensing suggests a division of labor in *Pseudomonas aeruginosa* populations. Elife 8:e45084. https://doi.org/10.7554/eLife.45084.
33. O'Neal L, Baraquet C, Suo Z, Dreifus JE, Peng Y, Raivio TL, Wozniak DJ, Harwood CS, Parsek MR. 2022. The Wsp system of *Pseudomonas aeruginosa* links surface sensing and cell envelope stress. Proc Natl Acad Sci U S A 119:e2117633119. https://doi.org/10.1073/pnas.2117633119.
34. Rice MS, Dahlquist FW. 1991. Sites of deamidation and methylation in Tsr, a bacterial chemotaxis sensory transducer. J Biol Chem 266:9746–9753. https://doi.org/10.1016/S0021-9258(18)92884-X.
35. Li Y, Hu Y, Fu W, Xia B, Jin C. 2007. Solution structure of the bacterial chemotaxis adaptor protein CheW from *Escherichia coli*. Biochem Biophys Res Commun 360:863–867. https://doi.org/10.1016/j.bbrc.2007.06.146.
36. da Re S, Tolstykh T, Wolanin PM, Stock JB. 2002. Genetic analysis of response regulator activation in bacterial chemotaxis suggests an intermolecular mechanism. Protein Sci 11:2644–2654. https://doi.org/10.1110/ps.0220402.
37. Bellsolell L, Prieto J, Serrano L, Coll M. 1994. Magnesium binding to the bacterial chemotaxis protein CheY results in large conformational changes involving its functional surface. J Mol Biol 238:489–495. https://doi.org/10.1006/jmbi.1994.1308.
38. Huangyutitham V, Güvener ZT, Harwood CS. 2013. Subcellular clustering of the phosphorylated WspR response regulator protein stimulates its diguanylate cyclase activity. mBio 4:e00242-13. https://doi.org/10.1128/mBio.00242-13.
39. Wei Q, Leclercq S, Bhasme P, Xu A, Zhu B, Zhang Y, Zhang M, Wang S, Ma LZ. 2019. Diguanylate cyclases and phosphodiesterases required for basal-level c-di-GMP in *Pseudomonas aeruginosa* as revealed by systematic phylogenetic and transcriptomic analyses. Appl Environ Microbiol 85:e01194-19. https://doi.org/10.1128/AEM.01194-19.
40. Fang X, Ahmad I, Blanka A, Schottkowski M, Cimdins A, Galperin MY, Römling U, Gomelsky M. 2014. GIL, a new c-di-GMP-binding protein domain involved in regulation of cellulose synthesis in enterobacteria. Mol Microbiol 93:439–452. https://doi.org/10.1111/mmi.12672.
41. Carman GM, Han GS. 2006. Roles of phosphatidate phosphatase enzymes in lipid metabolism. Trends Biochem Sci 31:694–699. https://doi.org/10.1016/j.tibs.2006.10.003.
42. Ricca E, Limauro D, Lago CT, de Felice M. 1988. Enhanced acetohydroxy acid synthase III activity in an *ilvH* mutant of *Escherichia coli* K-12. J Bacteriol 170:5197–5199. https://doi.org/10.1128/jb.170.11.5197-5199.1988.
43. Shannon P, Markiel A, Ozier O, Baliga NS, Wang JT, Ramage D, Amin N, Schwikowski B, Ideker T. 2003. Cytoscape: a software environment for integrated models of biomolecular interaction networks. Genome Res 13:2498–2504. https://doi.org/10.1101/gr.1239303.
44. Petelski AN, Fonseca Guerra C. 2019. Designing self-assembled rosettes: why ammeline is a superior building block to melamine. ChemistryOpen 8:134–134. https://doi.org/10.1002/open.201900001.
45. Reichhardt C, Wong C, da Silva DP, Wozniak DJ, Parsek MR. 2018. CdrA interactions within the *Pseudomonas aeruginosa* biofilm matrix safeguard it from proteolysis and promote cellular packing. mBio 9:e01376-18. https://doi.org/10.1128/mBio.01376-18.
46. Cooley RB, Smith TJ, Leung W, Tierney V, Borlee BR, O'Toole GA, Sondermann H. 2016. Cyclic di-GMP-regulated periplasmic proteolysis of a *Pseudomonas aeruginosa* type Vb secretion system substrate. J Bacteriol 198:66–76. https://doi.org/10.1128/JB.00369-15.
47. Borlee BR, Goldman AD, Murakami K, Samudrala R, Wozniak DJ, Parsek MR. 2010. *Pseudomonas aeruginosa* uses a cyclic-di-GMP-regulated adhesin to reinforce the biofilm extracellular matrix. Mol Microbiol 75:827–842. https://doi.org/10.1111/j.1365-2958.2009.06991.x.
48. Wehbi H, Portillo E, Harvey H, Shimkoff AE, Scheurwater EM, Howell PL, Burrows LL. 2011. The peptidoglycan-binding protein FimV promotes assembly of the *Pseudomonas aeruginosa* type IV pilus secretin. J Bacteriol 193:540–550. https://doi.org/10.1128/JB.01048-10.
49. Buendia L, Girardin A, Wang T, Cottret L, Lefebvre B. 2018. LysM receptor-like kinase and LysM receptor-like protein families: An update on phylogeny and functional characterization. Front Plant Sci 9:1531. https://doi.org/10.3389/fpls.2018.01531.
50. Soto SM. 2013. Role of efflux pumps in the antibiotic resistance of bacteria embedded in a biofilm. Virulence 4:223–229. https://doi.org/10.4161/viru.23724.
51. Liang F, Zhang B, Yang Q, Zhang Y, Zheng D, Zhang L, Yan Q, Wu X. 2020. Cyclic-di-GMP regulates the quorum-sensing system and biocontrol activity of *Pseudomonas fluorescens* 2P24 through the RsmA and RsmE proteins. Appl Environ Microbiol 86:e02016-20. https://doi.org/10.1128/AEM.02016-20.
52. Compeau G, Al-Achi BJ, Platsouka E, Levy SB. 1988. Survival of rifampin-resistant mutants of *Pseudomonas fluorescens* and *Pseudomonas putida* in soil systems. Appl Environ Microbiol 54:2432–2438. https://doi.org/10.1128/aem.54.10.2432-2438.1988.
53. Kirner S, Krauss S, Sury G, Lam ST, Ligon JM, van Pée KH. 1996. The non-haem chloroperoxidase from *Pseudomonas fluorescens* and its relationship to pyrrolnitrin biosynthesis. Microbiology 142:2129–2135. https://doi.org/10.1099/13500872-142-8-2129.
54. Matthews M, Roy CR. 2000. Identification and subcellular localization of the *Legionella pneumophila* IcmX protein: a factor essential for establishment of a replicative organelle in eukaryotic host cells. Infect Immun 68:3971–3982. https://doi.org/10.1128/IAI.68.7.3971-3982.2000.
55. Winsor GL, Griffiths EJ, Lo R, Dhillon BK, Shay JA, Brinkman FSL. 2016. Enhanced annotations and features for comparing thousands of *Pseudomonas* genomes in the *Pseudomonas* genome database. Nucleic Acids Res 44:D646–D653. https://doi.org/10.1093/nar/gkv1227.
56. Lu S, Wang J, Chitsaz F, Derbyshire MK, Geer RC, Gonzales NR, Gwadz M, Hurwitz DI, Marchler GH, Song JS, Thanki N, Yamashita RA, Yang M, Zhang D, Zheng C, Lanczycki CJ, Marchler-Bauer A. 2020. CDD/SPARCLE: the conserved domain database in 2020. Nucleic Acids Res 48:D265–D268. https://doi.org/10.1093/nar/gkz991.
57. Kim W, Levy SB. 2008. Increased fitness of *Pseudomonas fluorescens* Pf0-1 leucine auxotrophs in soil. Appl Environ Microbiol 74:3644–3651. https://doi.org/10.1128/AEM.00429-08.
58. Feng X, Lilly AA, Hazelbauer GL. 1999. Enhanced function conferred on low-abundance chemoreceptor Trg by a methyltransferase-docking site. J Bacteriol 181:3164–3171. https://doi.org/10.1128/JB.181.10.3164-3171.1999.
59. Alexander RP, Lowenthal AC, Harshey RM, Ottemann KM. 2010. CheV: CheW-like coupling proteins at the core of the chemotaxis signaling network. Trends Microbiol 18:494–503. https://doi.org/10.1016/j.tim.2010.07.004.
60. Malone JG, Williams R, Christen M, Jenal U, Spiers AJ, Rainey PB. 2007. The structure-function relationship of WspR, a *Pseudomonas fluorescens* response regulator with a GGDEF output domain. Microbiology (Reading) 153:980–994. https://doi.org/10.1099/mic.0.2006/002824-0.
61. O'Connor JR, Kuwada NJ, Huangyutitham V, Wiggins PA, Harwood CS. 2012. Surface sensing and lateral subcellular localization of WspA, the receptor in a chemosensory-like system leading to c-di-GMP production. Mol Microbiol 86:720–729. https://doi.org/10.1111/mmi.12013.